FISEVIER

Contents lists available at ScienceDirect

# **Chemical Physics Impact**

journal homepage: www.sciencedirect.com/journal/chemical-physics-impact



Full Length Article

# Radiation shielding study of tungsten impact on tellurite-bismuth based glasses

Kh.A. Bashar a, D, M.F.N. Jaafar , Y. Mansur , S.O. Baki b, M.A. Mahdi d

- <sup>a</sup> Department of Electrical Engineering Techniques, Faculty of Engineering, Al Manara University, Iraq
- <sup>b</sup> Department of Physics, Faculty of Science, Universiti Putra Malaysia, 43400, UPM, Serdang, Selangor, Malaysia
- <sup>c</sup> Physics Unit, Centre for Foundation Studies in Science, Universiti Putra Malaysia, 43400, UPM, Serdang, Selangor, Malaysia
- <sup>d</sup> Institute of Nanoscience and Nanotechnology, Universiti Putra Malaysia, 43400 Serdang, Selangor, Malaysia

#### ARTICLE INFO

#### Keywords: Tellurite Melt-quenching Radiation shielding Mass attenuation Exposure build factor

#### ABSTRACT

The current study, a new Pb-free glasses of host (H) and four samples (S1-S4) of tellurite-bismuth-tungsten oxide according to formula: (70-x) TeO<sub>2</sub>-10Bi<sub>2</sub>O<sub>3</sub>-10ZnO-10Al<sub>2</sub>O<sub>3</sub>- xWO<sub>3</sub>, x = 0, 5, 10, 15, 20 mol %, were prepared by traditional melt-quenching method. The phase formation of all samples is analyzed by XRD (x-ray diffraction) were found they are without any crystallization network. Some physical properties like density and molar volume were estimated as well. Within energy of 0.015MeV-15MeV, samples are investigated in terms of gamma ray radiation shielding features. The MCNP5 stimulation code and theoretical XCOM software in addition to the other relevant equations are implemented to determine the mass attenuation coefficient (MAC) values where the other parameters are identified depending on its value such as mean free path (MFP), effective atomic number (Zeff) and half-value layer (HVL). Also, the exposure build factor (EBF) and energy absorbed build factor (EABF) are evaluated by the geometric progression (G-P) fitting method. The appearance of synthesized glasses reflects that, the increment of WO<sub>3</sub> contents leads to increase the glasses opacity due to their density between 3.532 -3.912 g/cm<sup>3</sup>. The uncertainty concentrations of the samples are calculated were they emphasized the accuracy of glass compositions. Moreover, the calculation results of stimulated MCNP5 code and theoretical XCOM program are closely matched, as the difference between them can be neglected. Further, the comparison with other works is made which emphasized the enhancement of the findings. Finally, according to above merits and results, the effectiveness of the radiation shielding features can be obviously recognized which is due to the WO3 incorporated concentrations.

#### 1. Introduction

Nowadays, radiation shielding material glasses plays a crucial role in mitigation the negative impact of ionizing radiation like gamma and X-rays in addition to subatomic particles, such as electrons, neutrons, and alpha particles. Recently, borosilicate and borotellurite based glasses doped with rare-earth or heavy metals attracts the researcher's attention due to their properties and performance in various applications [1–5]. Also, there is more interest in developing an optimized radiation shielding materials against gamma rays and neutrons radiations [1–3]. Bismuth-tellurite glass takes place in this field where it proofs excellent shielding as well [6]. Actually, tellurite-based glasses are preferable due to their merits as they introduce low phonon energy, high refractive index, excellent durability and good thermal stability [7,35,37,39]. The

tellurite low phonon energy reduces the non-radiative transition probability which is in turn minimize the non-radiative energy [8,9]. Most importantly, tellurite glasses exhibit superior third-order optical non-linearity and ultrafast non-linear optical response in both its linear and non-linear optical (NLO) properties [7]. So, tellurite glasses are helpful for optical communication, non-linear optics and in laser applications [10]. Additionally, bismuth ( $Bi_2O_3$ ) heavy metal may function as conditional glass formers, and the possibility of forming a more stable glass increases with the inclusion of aluminum and zing [8]. Thus, to increase the tellurium oxide's ability of glass formation, modifier oxides such as alkali, alkaline, or heavy metal oxides must be added to the composition [2]. In fact, ZnO considered as transition metal oxide (TMO) as modifier which takes place in glass preparation [24]. Also, ZnO contributes to oxide glasses by extending their UV optical

E-mail addresses: basharabbass8@gmail.com (Kh.A. Bashar), sharudinomar@upm.edu.my (S.O. Baki).

<sup>\*</sup> Corresponding authors.

transparency and improving the glass-forming region in addition to the non-hygroscopic glass nature improvement.

The aluminum oxide (Al<sub>2</sub>O<sub>3</sub>) addition improves the chemical durability and mechanical strength [11]. As known, tungsten has remarkable radiation attenuation capabilities due to its high density and atomic number. According to the last paragraph, the importance of this study is coming up by developing a pb-free glass is due to the lead toxic properties. Also, tungsten metal (W) is included in our composition due to its attractive merits as it has high atomic number (74) and density of (19.250 g/cm<sup>3</sup>). Tungsten plays an important role in many applications like radiation shielding, super alloys, X-ray tubes, and light bulb filaments. Various studies have concentrated on figuring out how well the performance of W-based glasses in radiation shielding field [13]. Ersundu et al. [19] was examined the tungsten-molybdenum-tellurite radiation shielding at photon energies of 0.808, 0.2764, 0.3028, 0.356, and 0.3838 MeV. According to their findings, the glass sample encoded W10M10T80 exhibits the best gamma-ray attenuation performance. The Li<sub>2</sub>B<sub>4</sub>O<sub>7</sub>-Bauxite glass system was created by Kavaz et al. [14] in order to assess the glasses potentiality as radiation shielding materials. They claimed that the 40 % bauxite glass sample had the best neutron and gamma shielding capability. The binary and trinary glass system were produced by El-Mallawany et al. [33] where emphasized their capabilities of shielding the ionized radiations. Above studies and more has inspired us to carry out the research that we are currently doing. So, the purpose of this study is to produce a new Pb-free samples of tellurite-bismuth based glass systems. At the same time, to investigate the impact of tungsten metal on these glasses in terms of radiation shielding properties. This investigation is done by employing the necessary stimulation code and theoretical calculations software in addition to the comparison with other relevant work findings.

#### 2. Experimental

#### 2.1. Glass fabrication

Host (H) and four samples (S1-S4) of tellurite-bismuth-tungsten oxide: (70-x) TeO<sub>2</sub>-10Bi<sub>2</sub>O<sub>3</sub>-10ZnO-10Al<sub>2</sub>O<sub>3</sub>- xWO<sub>3</sub>, x = 0, 5, 10, 15, 20 mol %, were prepared by traditional melt-quenching method using analytical grade chemicals TeO<sub>2</sub>, Bi<sub>2</sub>O<sub>3</sub>, Al<sub>2</sub>O<sub>3</sub>, ZnO and WO<sub>3</sub> (Table 1). To create a batch of 20 g, the proper weights of the raw components were measured and thoroughly combined in an agate pestle and mortar. Also, to keep the composition molarity of 100 % one can observe that, the increasing of WO<sub>3</sub> molarity percentage facing decrement in TeO<sub>2</sub> content (see Table 1). At the same time, we optimize the cost of base glass former (TeO2) content as much as possible according to the glass transparency. The ramping rate of furnace to reach 930 Co is done in steps. Firstly, the furnace reaches 300 C<sup>o</sup> within one hour and keeping the armpit with this degree for a half hour. Then, reach the temperature of 900 C<sup>o</sup> with three hours and keeping it for 5 h to have time for samples preparation. For half an hour, the powder was heated to 930 C<sup>o</sup> in an alumina crucible. In order to achieve a uniform melt with bubbles free, the crucible was rocked repeatedly. After being cooled with room temperature, the melt was annealed for five hours at 300 C°. For the purpose of measurement, the final state of the samples is in powder and bulk form where they polished after cutting to 3 mm thickness with diameter

of 5 cm as illustrated in Fig. 2. The phone camera Samsung(S20+) of high resolution was used for samples image with specifications of Triple lenses (12 MP, 26 mm (wide), dual pixel PDAF, 1–3x hybrid optical zoom) and LED flash auto-HDR.

### 2.2. X-ray diffraction (XRD) and density investigations

Four samples of tungsten-bismuth-tellurite in addition to the host glass were subjected to X-ray diffraction (XRD) analysis. At room temperature, XRD spectra have been acquired from the Philips system. For glass samples, the patterns have been measured in the  $2\theta$  scan step from  $10^{\circ}$  to  $100^{\circ}$  (degree per minute).

#### 2.3. Density, molar volume and uncertainty

Glass sample densities  $(\rho)$  were measured using the Archimedes method as follows:

$$\rho = \frac{w_g}{w_o - w_l} \times \rho_l \tag{1}$$

Where  $w_g$ ,  $w_l$  and  $\rho_l$  are weight of the glass in air and liquid and density of liquid, respectively. Using measured density and molecular weight of i<sup>th</sup> oxides (M), the molar volume  $V_m$  of all glasses has been calculated as following:

$$V_m = \frac{\sum_i x_i M_i}{\rho} \tag{2}$$

Where,  $x_i$  is the mole fraction of each oxide and  $\rho$  is the density of the glass sample.

Moreover, the uncertainties of the sample concentrations are identified as following (Table 1).

The sample concentration c is defined as

$$c = \frac{m}{M.V} \tag{3}$$

where m is the mass, V is the volume and M is the molar mass of substance. Thus, the concentration uncertainty u(c) can be defined as:

$$\left(\frac{u(c)}{c}\right) = \sqrt{\left(\frac{u(m)}{m}\right)^2 + \left(\frac{u(M)}{M}\right)^2 + \left(\frac{u(V)}{V}\right)^2} \tag{4}$$

# 2.4. Radiation parameters measurements

Montecarlo code (MCNP5) stimulated code and XCOM program [15, 16] were employed to determine the radiation attenuation parameters by utilizing the mass attenuation coefficient (*MAC*) data according to the following equation [12].

$$MAC = \frac{Ln(I_o/I)}{\rho x} \tag{5}$$

Where,  $I_o$  and I are the photon intensity without absorber and intensity of transmitted photon, respectively.  $\rho$  and x are the densities and thickness of the prepared samples.

In present study, MCNP5 simulation code has been used to identify

Table 1
Glass composition, molar volume, density and uncertainty.

Glass	Composi	tions (mole %	n)			Molar Volume (cm3/mol)	Density (g/cm <sup>3</sup> )	Uncertainty $u(c)$ (mol*l <sup>-1</sup> ) *10 <sup>-7</sup>
	TeO <sub>2</sub>	$Bi_2O_3$	$Al_2O_3$	ZnO	WO <sub>3</sub>			
Н	70	10	10	10	0	30.071	3.061	1.4162
<b>S1</b>	65	10	10	10	5	30.204	3.532	1.3878
<b>S2</b>	60	10	10	10	10	30.337	3.816	1.3606
<b>S</b> 3	55	10	10	10	15	30.470	3.854	1.3344
<b>S4</b>	50	10	10	10	20	30.603	3.912	1.3092

the MAC of the samples where the input parameters are defined in the simulation file with consideration of composition properties and experimental setup. The geometrical forms of the samples in addition to the physical parameters are defined in the cell card and surface card of the simulation input file. The geometries of cylindrical form were implemented for our 4 samples with 3 mm thickness as can be shown in Fig. 1. The collimator and point source are putted on z-axis as the introduced to the data card of the MCNP5 in addition to the ERC commands of energy and particles type. To calculate the intensity of photon which related to gamma flux over the surface, point detector tally F2 was employed. Also, the material card of MCNP5 includes the weight of each element of glass composition. The performance of simulation is done with one million histories and the results are reported with error > 0.1 % percentage of the output file.

The mean free path (MFP), half-value layer (HVL) and effective atomic number ( $Z_{eff}$ ) are identified according to the following Eqs. (6, 7 and 8) [11].

$$MFP = \frac{1}{\mu} \tag{6}$$

$$HVL = \frac{0.693}{\mu} \tag{7}$$

$$Z_{eff} = \frac{\sum i f_i A_i \left(\frac{\mu}{\rho}\right)_i}{\sum j f_j \frac{A_j}{z_j} \left(\frac{\mu}{\rho}\right)_i}$$
(8)

Where  $z_j$  is the atomic number,  $f_i$  is the fractional abundance of the element "i",  $A_i$  is the atomic weight and  $\mu$  is the linear attenuation coefficient and equal to  $(\mu/\rho$  \* density) of the glasses. The theoretical mass attenuation coefficient  $(\mu m)$  values are obtained through XCOM software of the glasses [16].

Exposure build factor (EBF) and exposure absorbed build factor (EABF) are identified within energy range of 0.015MeV-15MeV as the approach of G-P fitting parameters are identified in order to reflect the radiation properties of prepared glasses [21].

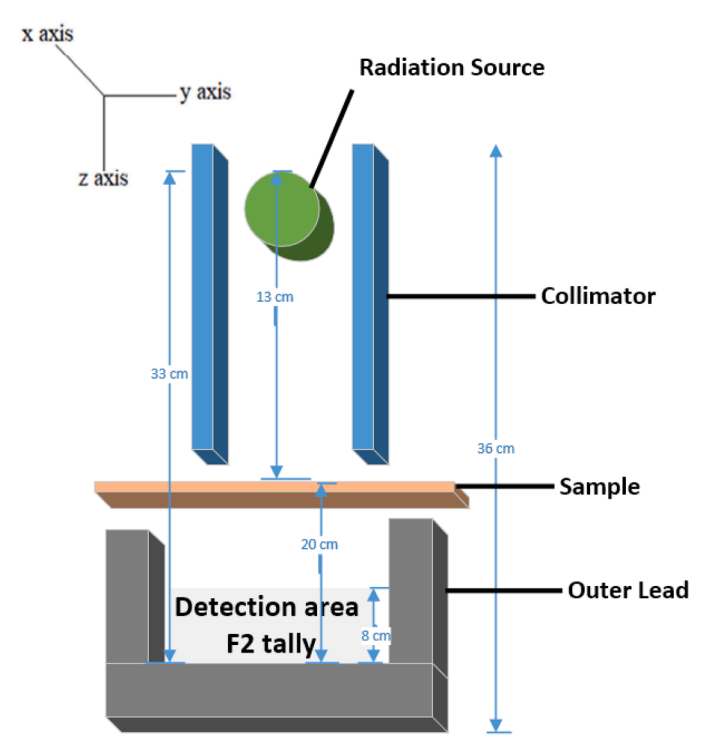


Fig. 1. Simulation geometry of MCNP5 with dimensions.

Regarding to EBF calculation where the scattered – radiation affects the beam detector; thus, the transmitted beam intensity could be calculated by the modified Lambert–Beer's law as following Eq. (9) [17]:

$$EBF = \left[ \left( \mu_{th} - \mu_{exp} \right) t \right] \tag{9}$$

#### 3. Results and discussion

Chemical compositions details of the studied glasses with the molar volumes, densities and uncertainty are given in Table 1. Glance on this table, one can say that the density increases with the increase of  $WO_3$  content from 0 to 20 mol %. Also, the range of density is in good agreement with tellurite glass systems reported by [18,19]. In fact, the atomic weight and molar volume of the constituent oxides are affecting the compositions density of the glasses in addition to their molecular weight. The molar volume in the same table is determined by using Eq. (2), where increased from 30.071 to 30.603 cm³/mol. Furthermore, the concentration uncertainty is calculated which is emphasize the high accuracy of the calculations and identifications of densities, molar mass in addition to the molar volume of the glasses.

Fig. 3 shows the XRD patterns for present samples (H, S1–S4) within range of  $20 \le 2\theta \le 80$  in  $2\theta$  scan with CuK $\alpha$  as a target and Ni as a filter in  $2^{\circ}$  /min scanning step.

It's clear that, the glass profiles are clear from the continuous or discrete sharp crystalline peaks. At the same time, the XRD profiles exhibit a broadly diffused scattering from  $25^{\circ}$  to  $50^{\circ}$ , which indicates the structural disorder for the glasses. One can notice that in H sample profile which is WO $_3$  free content, has more prominent peak at 25 degrees comparing with other samples being more boarded. That's due to the WO $_3$  contribution increment in (S1-S4) glasses and the decrement of the TeO $_2$ , which affect the glass matrix (please see Table 1). Also, it's worthy to mention that there is no any shift or deviation is recognized in the hump's profiles of present glasses. Upon above one can say that, theses samples have amorphous nature.

#### 3.1. Mass attenuation coefficients (MAC)

The mass attenuation coefficient parameter is the base one where the other shielding parameters are calculated through its value. This parameter can be calculated through deferent software, such as phy-x program, XCOM and MNCP5 code simulation [16,20].

The last code is implemented to identify the shielding parameter starting with MAC of the present glasses with energy range of 0.015 – 15MeV [22–24]. The MNCP5 setup and details already mention in previous section (2.4). Furthermore, The XCOM code was utilized to highlight the simulated outcomes and to emphasize the MNCP5 results. The variation of MAC of the synthesized glasses within above energy range according to the composition changes are shown in Fig. 4.

At the same time, the Monte Carlo simulation program (MCNP5) and the XCOM code findings of the synthesized glasses are presented in Table 2 (please see supplementary material file). The error difference of MAC values between the two codes is calculated through the following equation:

$$Diff(\%) = \frac{MCNP(value) - XCOM(value)}{XCOM(value)} \times 100\%$$
 (10)

From Table 2, the researchers can obviously recognize that, the MCNP5 code results are very closed to the XCOM data. In fact, this small difference is due to the mathematical rendering. Also, both of them are uses the same input data. So, the differences are coming from the code performance ability as each of them store the calculations to different decimal places, often 12 or 14 depending on their accuracy. Therefore, the calculations will be a bit different. Further, this closeness of findings can be found in many reported works [36,38]. So, we can conclude that the results in the current work accurately gives the MAC values of the



Fig. 2. Glass samples images.

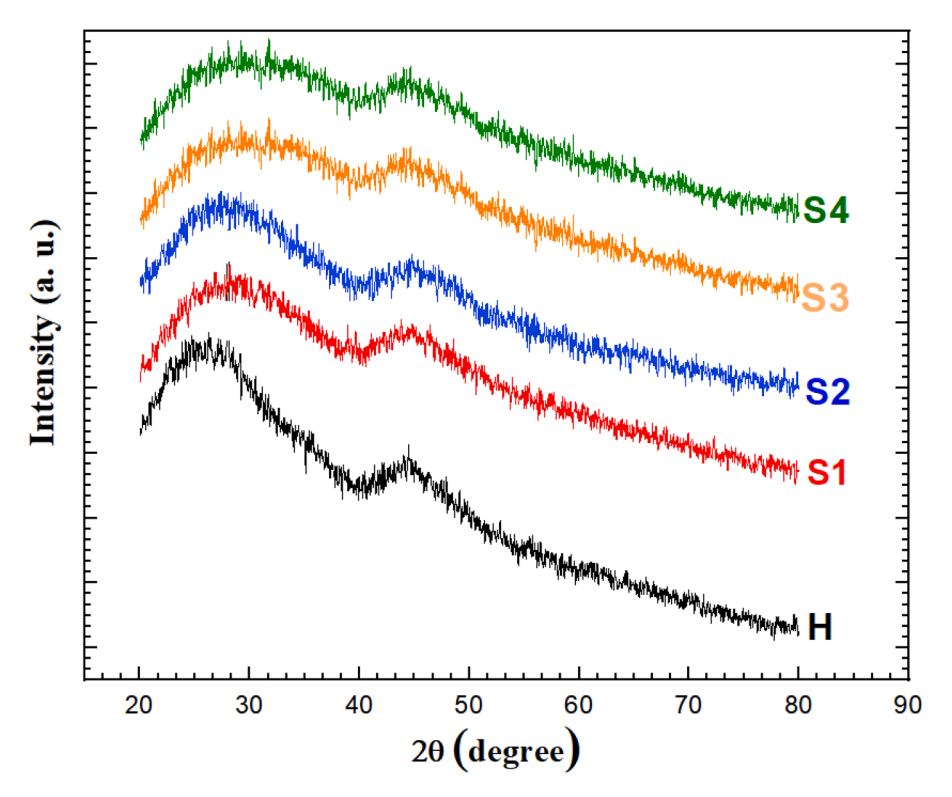


Fig. 3. X-ray diffraction patterns of the prepared glasses.

samples (S1-S4). According to Fig. 4 (inset fig) and Table 2, the MAC values for all synthesized glasses have the maximum level at 0.015 MeV photon energy and S4 is the heights. Above 0.015 MeV, values, the quick reduction is clear for all glass due to the photoelectric interaction (PE) [24].

At 0.07 MeV, values of the MAC for all synthesized glasses suffered a quietly reduction where the interaction of Compton scattering (CS) takes place as its interaction cross section inversely proportional to photon energy. Also, the mass attenuation for the samples is constant due to the pair creation (PC) [24]. Moreover, it's clear that the K-absorption edge causes the sharp peak for the sample's patterns in the low region of energy precisely on 0.7 MeV. Upon all above, one can say that the increment of the WO $_3$  contents improve the MAC value of the fabricated glasses where the S4 (20 mol %) has the heights value among all glasses within energy variation.

# 3.2. Effective atomic number ( $Z_{eff}$ )

The effective atomic number ( $Z_{eff}$ ) patterns for the present glasses within 0.015–15 -MeV photon energy range is illustrated in Fig. 5 and its inset figure. It's clear that the curves trend is consistent with the reported  $Z_{eff}$  values in Ref. [25].

Also, it can be observed that, the  $Z_{eff}$  parameter of the glasses has the largest value in low energy range especially at 0.03 MeV then quickly reduced with energy increasing till 0.06 MeV to jump suddenly again and made another sharp edge at 0.1 MeV. These changes are due to the photon interaction with the heavy metals.

In fact, the sharp edge around 0.1 MeV as seen in inset figure where  $Z_{eff}$  got increases is attributed to the photoelectric effect around the k-absorption of the heavy metals [26]. Thereafter, in the energy range 0.15 - 1.5 MeV, the  $Z_{eff}$  value sharply decrease as the energy increase. This phenomenon is due to the dominance effect of the photoelectric process in the low energy region. Following the same figure, the  $Z_{eff}$  value increased again above 1.5 MeV and up to 15 MeV since the pair production process takes place in the higher energy region. It is important to note that the S4 glass sample has the highest value of  $Z_{eff}$  among all samples where it has the highest  $WO_3$  content.

# 3.3. Half value layer (HVL) and mean free path (MFP)

The HVL value identify the thickness of shielding material which reduce the initial incident photon energy to 50 % percent [2]. This value is calculated as mentioned earlier through Eq. (7). At the same time, the effective shielding can be done with the lower MFP value which can be

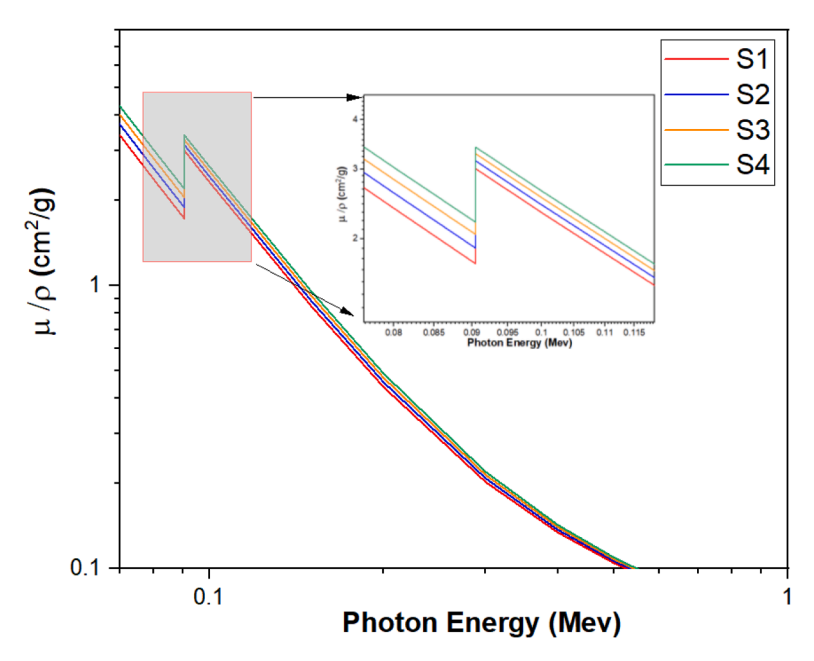


Fig. 4. Mass attenuation coefficients (MAC) for all glasses.

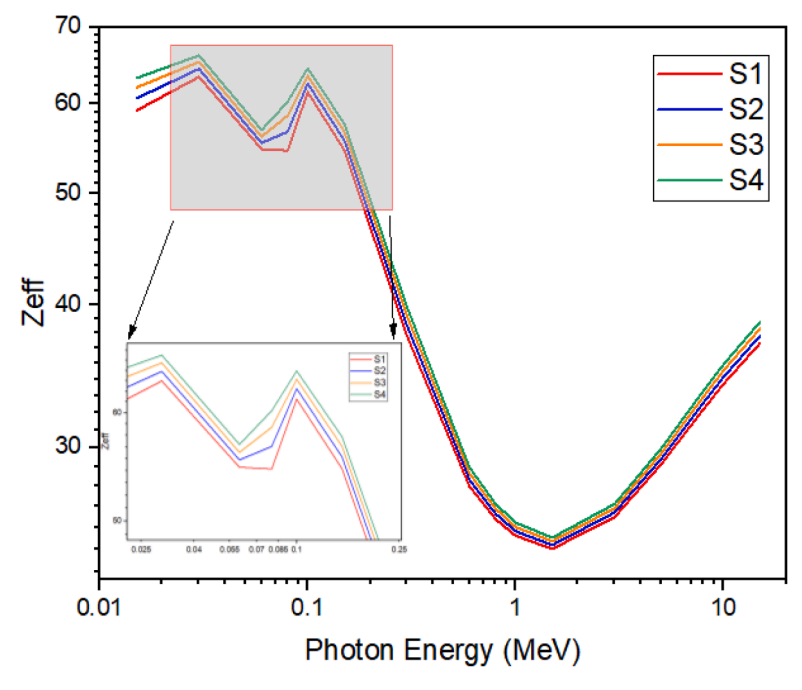


Fig. 5. Effective atomic number ( $Z_{\text{eff}}$ ) patterns for all glasses.

identified by Eq. (6). So, both of these parameters reflect superior shielding effect with their lowest values. In the current work, the HVL and MFP are calculated to comprehend the characteristics of radiation shielding for the present glasses S1-S4. The profiles of prepared glasses regarding these parameters are depicted in Fig. 6 and Fig. 7. Following the figures, it is clear that their values are depends on the chemical composition of the samples and incident photon energy as well. Further, one can observe that, the HVL and MFP findings are decrease with increasing of WO<sub>3</sub> content and increase with increasing of energy especially at 1- 6 MeV range. These changes are happened due to the sample's densities increment which are proportional to the increment of WO<sub>3</sub> concentrations.

In order to investigate the effectiveness of the prepared glasses (S1, S2, S3 and S4) from point of gamma ray shielding, the comparison of

their HVL values were made with other works after justifying their results (see Fig. 8). In fact, the comparison was made with lead glasses (S $_{1}$ , 2) of work Ref. [27] in addition to concrete samples (4, 5 and 6) of work Ref. [28] at energy interval (0.123–1.33) MeV. It is clear that HVL results are increased proportionally to the photon energy increment. At the same time, the concrete HVL values are higher than all glasses while our present samples have the lower values especially S3 and S4 glasses, as depicted in Fig. 8.

Thus, it is evident that the shielding capability of our glasses (S3 and S4) is higher than others glasses at 0.123-1.33MeV Energy range as they possess low HVL values.

Furthermore, to authenticate the shielding performance of present glasses, the comparison of MFP values is made with the same other works mentioned in previous paragraph at photon energy range of

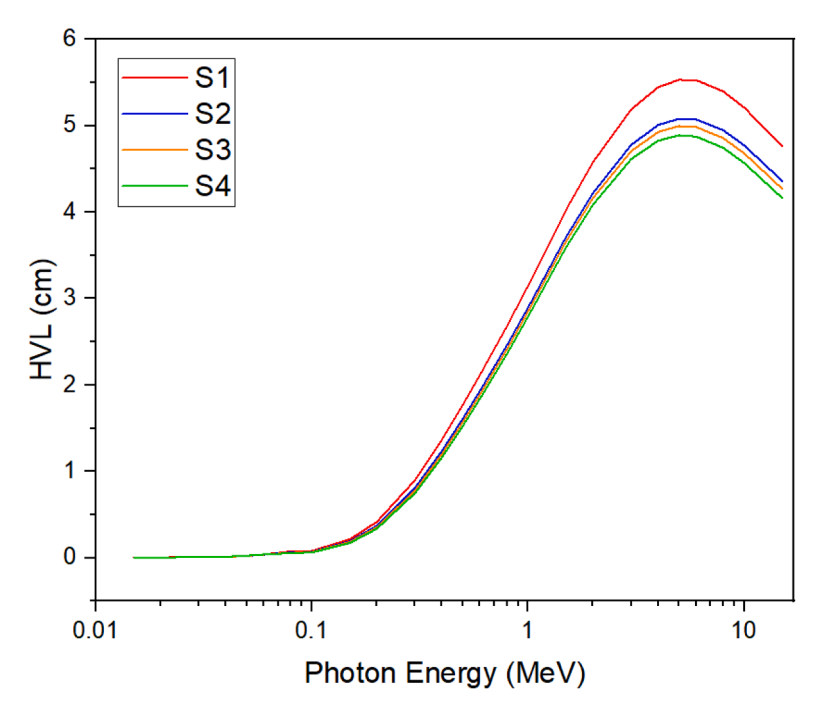


Fig. 6. Variation of HVL as a function of energy for all glasses.

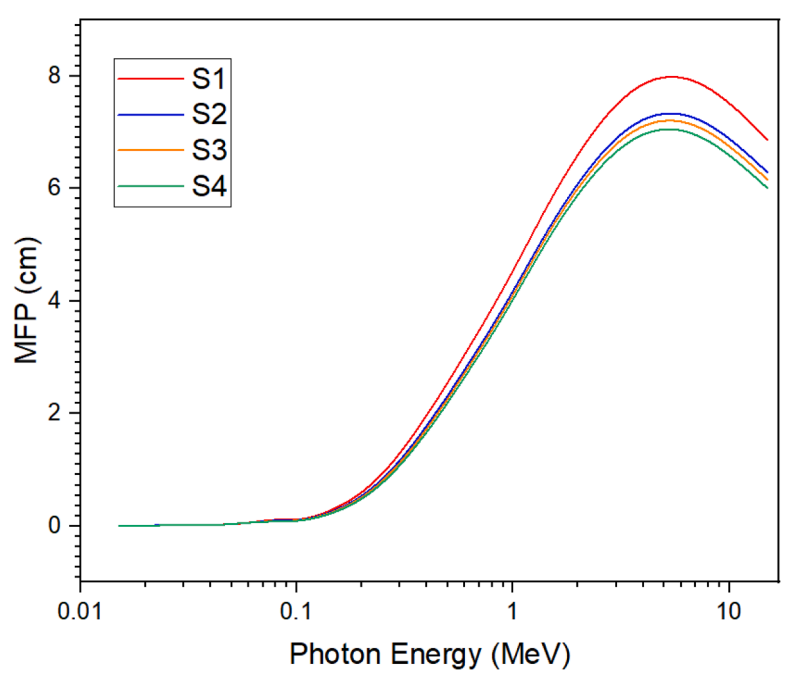


Fig. 7. Variation of MFP as a function of energy for all glass samples.

(0.123-1.33) MeV, as plotted in Fig. 9. The MFP values of samples  $(S_{1,2})$  of work [27] are lower than present glasses (S1 and S2), especially at energy range (0.1-1) MeV, while S3 and S4 present glasses possess lower MFP values than the other work samples (see Fig. 9) where they reflect superior radiation shielding among other glasses.

# 3.4. Exposure and energy absorbed buildup factor (EBF and EABF)

In general, the ratio of the total number of photons at any medium to the number of photons entering that environment independently is known as the buildup factor (EBF and EABF) [29].

EBF is the degree to which the material is exposed to the incoming

photons while the EABF represents the absorbed energy in the material which interacting with the incident photon. These parameters are identified with the Geometric Progression (G-P) fitting method which explained in many studies [30–32]. Figs. 10 and 11 display both (EBF and EABF) buildup factor against gamma- ray energy with deferent penetration depths (1, 5,10,20,30, 40) mfp. A glance on these figures, one can recognize three zones of buildup factors regarding to the energy (low, intermediate, and high). In these figures the S1 and S4 glasses of the current work are chosen as they represent the minimum and maximum values of WO<sub>3</sub> contents.

Regarding to these figures, one can observe that the EABF and EBF patterns possess quite low values at low energy range. In this region, the

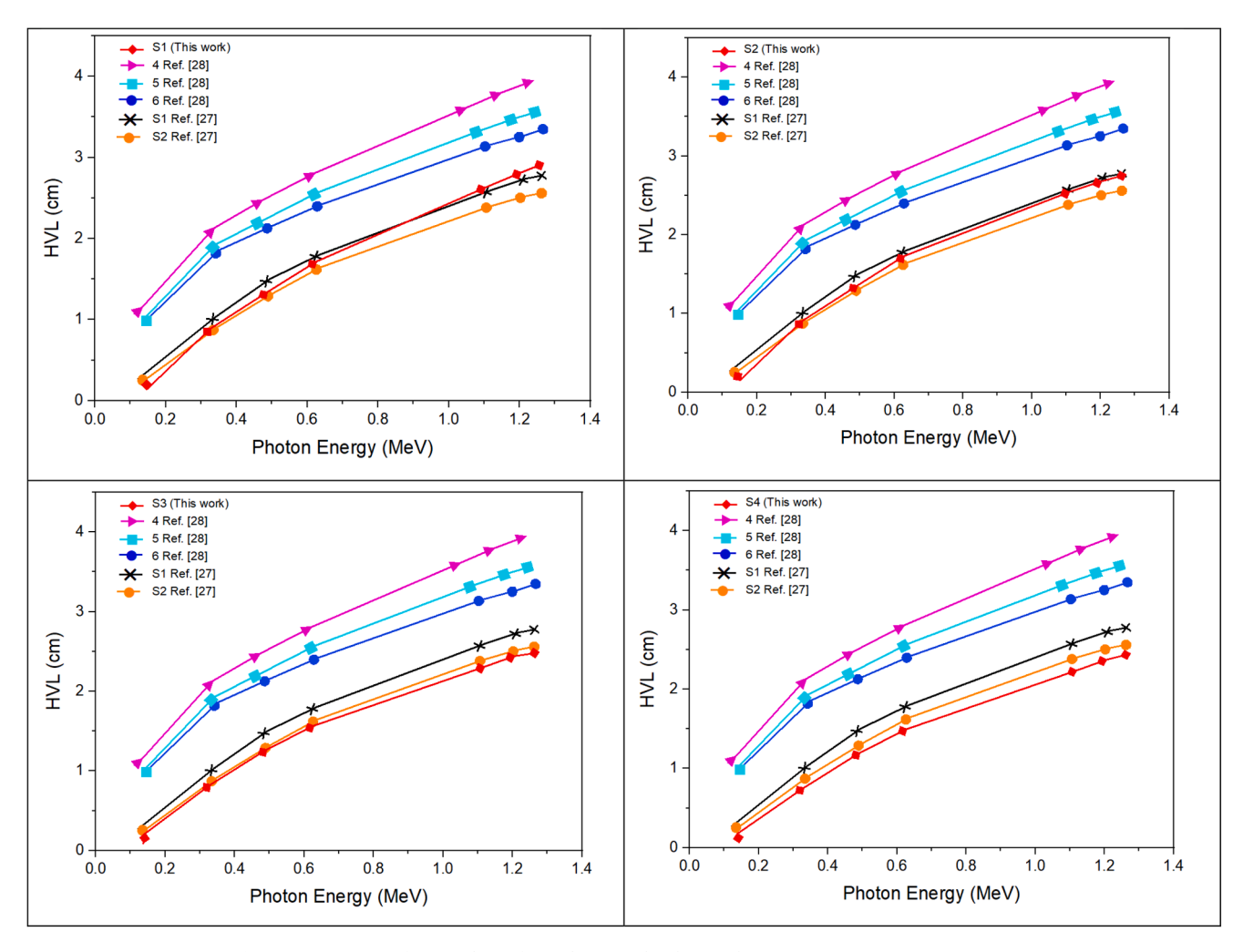


Fig. 8. Comparison of HVL values of our glasses with other works at 0.123–1.33MeV Energy range.

photons almost are absorbed completely due to the photoelectric effect which cause the less values of the buildup factors. Further, around 0.07 MeV in Fig. 10 there are very sharp peaks for S1 sample where they disappear for S4 glass due to the increment of  $WO_3$  content. At the same time this raise is related to the K-absorption edge process [25].

After 0.15 MeV, EBF and EABF values are increases gradually to the maximum value at energy of 2 MeV. In other word, with intermediate photon energy, the Compton scattering is the major process of interaction which assist the degradation of photon energy and leads to remove the photon completely [34]. So, the probability of photon to escape the material is related to its long life. This mechanism affects the values of the EBF and EABF to be higher.

It is known that, the effect of secondary scatterings being high in the middle energy range which is leads to increase the number of photons to buildup factor. So, the EBF and EABF values are related proportionally to the penetration depth enhancement where the increasing in MFP leads to more scattering. Moreover, there is swiftly grown of buildup factors at high range of energy and large penetration depth (20–40 mfp), due to the changing in pair production mechanism (PP). Consequently, one can distinguish a steep increment or sharp peaks at high energy ( $\sim$ 10 MeV) in addition to large penetration depth. This is due to the photons of secondary gamma were produced by electron – positron annihilation in the medium due to the multiple scattering process. Finally, upon the Figs. 10 and 11 the EBF and EABF values are decrease as the WO $_3$  contents increasing, thus, the S4 glass values of these parameters are lower than S1 glass as it has highest effective atomic number ( $Z_{\rm eff}$ ) among all samples.

#### 4. Conclusion

In this research, the radiation shielding parameters of new composition (70-x)  $TeO_2-10Bi_2O_3-10ZnO-10Al_2O_3$ -  $xWO_3$ , x=0, 5, 10, 15, 20mol %, Pb free glasses (H, S1-S4) were examined. The uncertainty concentrations of the samples are calculated were they emphasized the accuracy of glass compositions. For these glasses, the MCNP-5 code simulation was employed to evaluate the MAC values. These findings are compared with the theoretical results of XCOM software which reflect neglectable differences. With implementation of MAC values upon energy range of (0.015-15) MeV, other shielding parameters (Zeff, HVL, MFP, EBF and EABF) are utilized. The lead glass (S<sub>1, 2</sub> of work Ref. [27]) and concrete (4, 5 and 6 of work Ref. [28]) samples are chosen for the comparison with the current study results at energy interval (0.123-1.33) MeV. Regarding to HVL values, our present samples have lower values especially S3 and S4 glasses as they possess low HVL values. The same comparison of MFP is made with aforementioned other works which reflect that, the samples  $(S_{1,2})$  of work  $\[ 27 \]$  are lower than our glasses (S1 and S2), especially at energy range (0.1-1) MeV, while S3 and S4 glasses possess lower MFP values than the other work samples. The last two samples are showing superior radiation shielding. Further, a glance on the EBF and EABF findings of our glasses with minimum and maximum contents of WO<sub>3</sub> of S1 and S4 samples respectively, it's clear that the S4 sample possess lower value. Consequently, we can say that the S4 sample with highest WO<sub>3</sub> content and lowest TeO<sub>2</sub> concentration is achieved the highest absorption of gamma photons with low transparency advantage of visible light. On that, the contribution of WO3

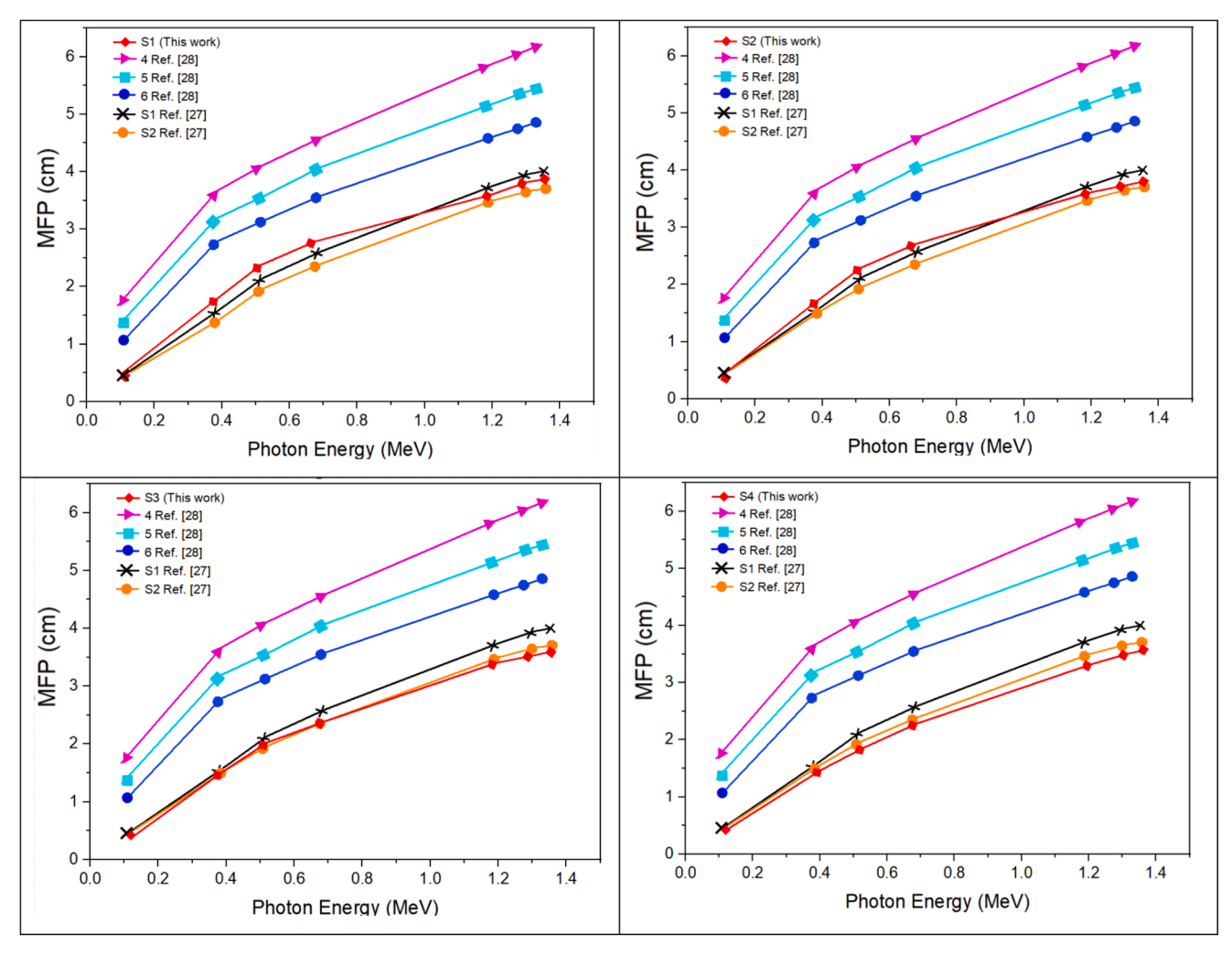


Fig. 9. Comparison of MFP values of our glasses with other works at 0.123-1.33MeV Energy range.

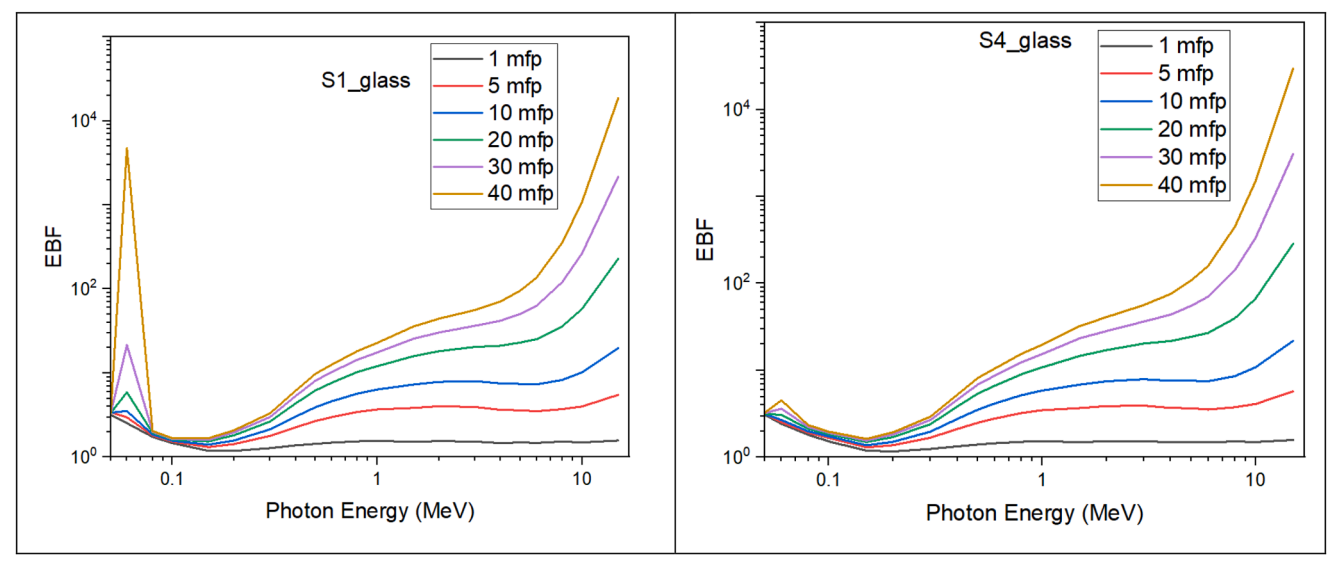


Fig. 10. Variations of the (EBF) for S1 and S4 glasses with photon energy at different penetration depths.

concentration to the examined glasses enhancing their nuclear protective features and can be considered as potential candidate for radiation shielding purposes.

# CRediT authorship contribution statement

Kh.A. Bashar: Writing – original draft, Methodology,

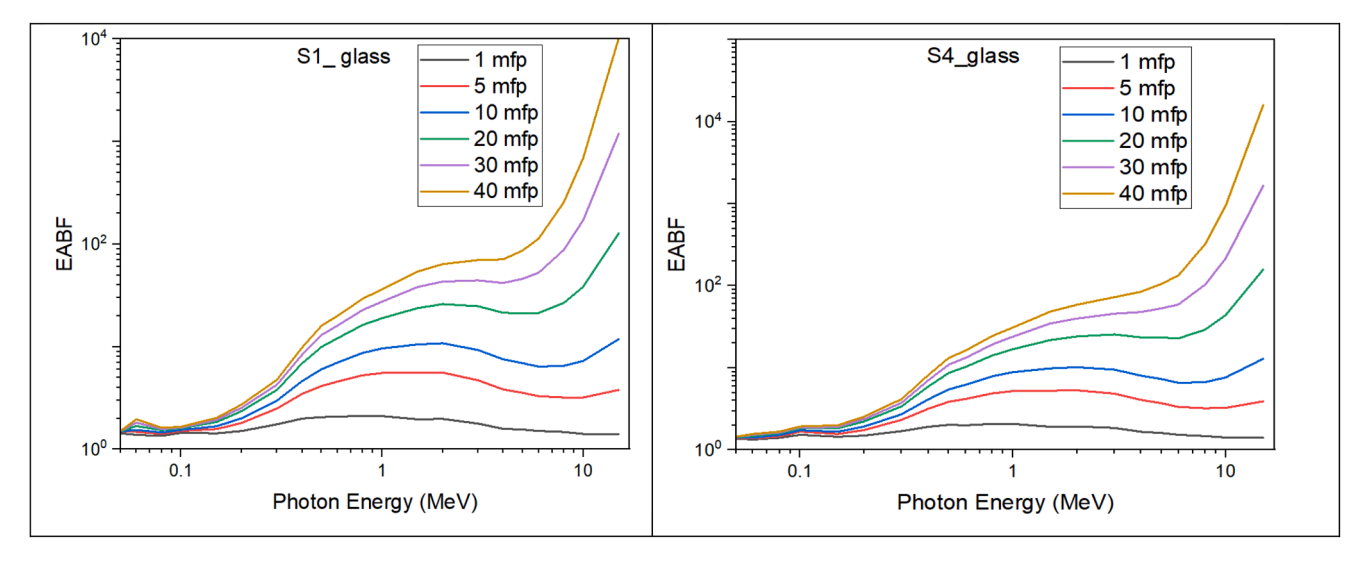


Fig. 11. Variations of the (EABF) for S1 and S4 glasses with photon energy at different penetration depths.

Conceptualization. M.F.N. Jaafar: Data curation. Y. Mansur: Formal analysis. S.O. Baki: Funding acquisition, Conceptualization. M.A. Mahdi: Resources, Project administration.

#### Declaration of competing interest

The authors declare that none of the work reported in this study could have been influenced by any known competing financial interests or personal relationships.

#### Acknowledgments

The authors would like to deeply thank UPM University-Malaysia for its support and funding under Geran Putra Berimpak (GPB/2021/9707700) by which this research could be conducted successfully.

#### Supplementary materials

Supplementary material associated with this article can be found, in the online version, at doi:10.1016/j.chphi.2025.100894.

# Data availability

Data will be made available on request.

# References

- [1] Kh A. Bashar, W.L. Fong, Kh A. Haider, S.O. Baki, M.H.M. Zaid, M.A. Mahdi, Optical studies on Tb3+: Dy3+ singly and doubly doped borosilicate glasses for white light and solid state lighting applications, J. Non Cryst. Solids 534 (2020) 119943.
- [2] Muhammad Fakhrul Naim Jaafar, Bashar Khudhair Abbas, Sharudin Omar Baki, Yaakob Mansor, Muhammad Khalis Abdul Karim, Mohd Adzir Mahdi, Radiation shielding study of heavy metal oxide bismuth-tungsten borate based glasses for defense and medical applications, J. Adv. Res. Appl. Sci. Eng. Technol. (2024) 268-275.
- [3] G. Lakshminarayana, Kh A. Bashar, S.O. Baki, A. Lira, U. Caldiño, A.N. Meza-Rocha, C. Falcony, E. Camarillo, I.V. Kityk, M.A. Mahdi, Er3+/Dy3+ codoped B2O3-TeO2-PbO-ZnO-Li2O-Na2O glasses: optical absorption and fluorescence features study for visible and near-infrared fiber laser applications, J. Non Cryst. Solids 503 (2019) 366–381.
- [4] Al-BFA Mohammed, G. Lakshminarayana, S.O. Baki, Kh A. Bashar, I.V. Kityk, M. A. Mahdi, Optical and dielectric studies for Tb3+/Sm3+ co-doped borate glasses for solid-state lighting applications, Opt. Mater. 86 (2018) 387–393.
- [5] Kh A. Bashar, G. Lakshminarayana, S.O. Baki, Al-BFA Mohammed, U. Caldiño, A. N. Meza-Rocha, Vijay Singh, I.V. Kityk, M.A. Mahdi, Tunable white-light emission from Pr3+/Dy3+ co-doped B2O3-TeO2 PbO-ZnO Li2O-Na2O glasses, Opt. Mater. 88 (2019) 558-569.

- [6] W.L. Fong, Kh.A. Bashar, S.O. Baki, M.K.A. Karim, M.I. Sayyed, M.A. Mahdi, B. T. Goh, O.B. Aljewaw, Influence of Bi2O3 content on structural, optical and radiation shielding properties of transparent Bi2O3-Na2O-TiO2-ZnO-TeO2 glass ceramics, Radiat. Phys. Chem. 200 (2022) 110289.
- [7] W.L. Fong, Kh A. Bashar, S.O. Baki, M.H.M. Zaid, B.T. Goh, M.A. Mahdi, Thermal, structural and optical properties of Bi2O3-Na2O-TiO2-ZnO-TeO2 glass system, J. Non Cryst. Solids 555 (2021) 120621.
- [8] Kresimir Furic, Masa Rajic-Linaric, C.S. Ray, A. Šantić, Andrea Moguš-Milanković, D.E. Day, Struct. Prop. Cryst. Sodium Tellurite Glas. (2008).
- [9] Virginie Nazabal, S. Todoroki, A. Nukui, T. Matsumoto, S. Suehara, T. Hondo, T. Araki, S. Inoue, Clara Rivero, Thierry Cardinal, Oxyfluoride tellurite glasses doped by erbium: thermal analysis, structural organization and spectral properties, J. Non Cryst. Solids 325 (1–3) (2003) 85–102.
- [10] W.L. Fong, Sharudin Omar Baki, N.M. Arifin, Yaakob Mansor, Ahmad Nazri, Bashar Khudhair Abbas, Structural, thermal and optical properties of rare earth doped lead tellurite oxide glasses, J. Adv. Res. Fluid Mech. Therm. Sci. 81 (2) (2021) 52–58.
- [11] Bashar Khudhair Abbas, Sharudin Omar Baki, Fong Wai Leng, Haider Khudhair Abbas, Layth Al-Sarraj, Mohd Adzir Mahdi, Investigation of structural, thermal properties and shielding parameters of borosilicate glasses doped with Dy3 +/Tb3+ ions for gamma and neutron radiation shielding applications, J. Adv. Res. Fluid Mech. Therm. Sci. 80 (1) (2021) 50–61.
- [12] Mohamed Amin Mahmoud Uosif, A.M.A. Mostafa, Shams AM Issa, H.O. Tekin, Z. A. Alrowaili, O.J.J.O.N.C.S. Kilicoglu, Structural, mechanical and radiation shielding properties of newly developed tungsten lithium borate glasses: an experimental study, J. Non Cryst. Solids 532 (2020) 119882.
- [13] A.E. Ersundu, M. Büyükyıldız, M.Çelikbilek Ersundu, Erdem Şakar, M.J.P.N. E. Kurudirek, The heavy metal oxide glasses within the WO3-MoO3-TeO2 system to investigate the shielding properties of radiation applications, Prog. Nucl. Energy 104 (2018) 280–287.
- [14] Esra Kavaz, H.O. Tekin, N. Yıldız Yorgun, Ö.F. Özdemir, M.I. Sayyed, Structural and nuclear radiation shielding properties of bauxite ore doped lithium borate glasses: experimental and Monte Carlo study, Radiat. Phys. Chem. 162 (2019) 187–193.
- [15] Shams AM Issa, Yasser B. Saddeek, H.O. Tekin, M.I. Sayyed, Khamies saber Shaaban, Investigations of radiation shielding using Monte Carlo method and elastic properties of PbO-SiO2-B2O3-Na2O glasses, Curr. Appl. Phys. 18 (6) (2018) 717–727.
- [16] Martin J. Berger, John Howard Hubbell, XCOM: Photon Cross Sections On a Personal computer. No. NBSIR-87-3597. National Bureau of Standards, Washington, DC (USA), Center for Radiation Research, 1987.
- [17] Necati Çelik, Uğur Çevik, Ahmet Çelik, Effect of detector collimation on the measured mass attenuation coefficients of some elements for 59.5–661.6 keV gamma-rays, Nucl. Instrum. Methods Phys. Res. B 281 (2012) 8–14.
- [18] Y. Gandhi, I.V. Kityk, M.G. Brik, P.Raghava Rao, N. Veeraiah, Influence of tungsten on the emission features of Nd3+, Sm3+ and Eu3+ ions in ZnF2–WO3–TeO2 glasses, J. Alloys Compd. 508 (2) (2010) 278–291.
- [19] D.K. Gaikwad, M.I. Sayyed, Shamsan S. Obaid, Shams AM Issa, P.P. Pawar, Gamma ray shielding properties of TeO2-ZnF2-As2O3-Sm2O3 glasses, J. Alloys Compd. 765 (2018) 451–458.
- [20] Erdem Şakar, Özgür Fırat Özpolat, Bünyamin Alım, M.I. Sayyed, Murat Kurudirek, Phy-X/PSD: development of a user friendly online software for calculation of parameters relevant to radiation shielding and dosimetry, Radiat. Phys. Chem. 166 (2020) 108496.
- [21] Yoshiko. Harima, An historical review and current status of buildup factor calculations and applications, Radiat. Phys. Chem. 41 (4–5) (1993) 631–672.
- [22] M.S. Gaafar, S.Y. Marzouk, H.A. Zayed, L.I. Soliman, A.H. Serag El-Deen, Structural studies and mechanical properties of some borate glasses doped with different alkali and cobalt oxides, Curr. Appl. Phys. 13 (1) (2013) 152–158.

- [23] Akshaykumar Salimath, Bahniman Ghosh, Effect of electric field and magnetic field on spin transport in bilayer graphene armchair nanoribbons: a Monte Carlo simulation study, Curr. Appl. Phys. 14 (11) (2014) 1526–1530.
- [24] Y.S. Rammah, F.I. El-Agawany, K.A. Mahmoud, R. El-Mallawany, Erkan Ilik, Gokhan Kilic, FTIR, UV-Vis-NIR spectroscopy, and gamma rays shielding competence of novel ZnO-doped vanadium borophosphate glasses, J. Mater. Sci. 31 (12) (2020) 9099–9113.
- [25] Y.S. Rammah, K.A. Mahmoud, Esra Kavaz, Ashok Kumar, F.I. El-Agawany, The role of PbO/Bi2O3 insertion on the shielding characteristics of novel borate glasses, Ceram. Int. 46 (15) (2020) 23357–23368.
- [26] A.M.A. Mostafa, Shams AM Issa, M.I. Sayyed, Gamma ray shielding properties of PbO-B2O3-P2O5 doped with WO3, J. Alloys Compd. 708 (2017) 294–300.
- [27] Narveer Singh, Kanwar Jit Singh, Kulwant Singh, Harvinder Singh, Gamma-ray attenuation studies of PbO–BaO–B2O3 glass system, Radiat. Meas. 41 (1) (2006) 84–88.
- [28] Issa, Shams AM, A.M.A. Mostafa, Effect of Bi2O3 in borate-tellurite-silicate glass system for development of gamma-rays shielding materials, J. Alloys Compd. 695 (2017) 302–310.
- [29] Berna Oto, Sinem Erden Gulebaglan, Zekiye Madak, Esra Kavaz, Effective atomic numbers, electron densities and gamma rays buildup factors of inorganic metal halide cubic perovskites CsBX3 (B= Sn, Ge; X= I, Br, Cl), Radiat. Phys. Chem. 159 (2019) 195–206.
- [30] Yorgun, Nergiz Yıldız, Esra Kavaz, Gamma photon protection properties of some cancer drugs for medical applications, Results Phys. 13 (2019) 102150.

- [31] Neslihan Ekinci, Esra Kavaz, Bünyamin Aygün, Ufuk Perişanoğlu, Gamma ray shielding capabilities of rhenium-based superalloys, Radiat. Eff. Defects Solids 174 (5–6) (2019) 435–451.
- [32] Mohammed Sultan Al-Buriahi, Baris T. Tonguc, Study on gamma-ray buildup factors of bismuth borate glasses, Appl. Phys. A 125 (7) (2019) 482.
- [33] R. El-Mallawany, M.I. Sayyed, M.G. Dong, Comparative shielding properties of some tellurite glasses: part 2, J. Non Cryst. Solids 474 (2017) 16–23.
- [34] S.R. Manohara, S.M. Hanagodimath, Leif Gerward, Energy absorption buildup factors for thermoluminescent dosimetric materials and their tissue equivalence, Radiat. Phys. Chem. 79 (5) (2010) 575–582.
- [35] N. Elkhoshkhany, Rafik Abbas, R. El-Mallawany, S.F. Hathot, Optical properties and crystallization of bismuth boro-tellurite glasses, J. Non Cryst. Solids 476 (2017) 15–24.
- [36] F.I. El-Agawany, K.A. Mahmoud, Esra Kavaz, R. El-Mallawany, Y.S. Rammah, Evaluation of nuclear radiation shielding competence for ternary Ge–Sb–S chalcogenide glasses, Appl. Phys. A 126 (2020) 1–11.
- [37] R. El-Mallawany, Samir Y. Marzouk, M.S. Gaafar, I.S. Mahmoud, Elastic and spectroscopic properties of 0.7 TeO 2–0.1 ZnO–0.1 NaF–(0.1–x) WO 3– x Nd 2 O 3 tellurite glasses, Indian J. Phys. 94 (2020) 1633–1641.
- [38] Gunha, Jaqueline Valeski, Robson Ferrari Muniz, Aloisi Somer, Simone do RF Sabino, Daniele Toniolo Dias, R. El-Mallawany, Andressa Novatski, The effect of fluorine replacement on the physical properties of oxyfluorotellurite glasses TeO2-Li2O-ZnO-ZnF2, J. Non Cryst. Solids 603 (2023) 122083.
- [39] M.N. Azlan, M.K. Halimah, A.B. Suriani, Y. Azlina, R. El-Mallawany, Electronic polarizability and third-order nonlinearity of Nd3+ doped borotellurite glass for potential optical fiber, Mater. Chem. Phys. 236 (2019) 121812.